Research on Duct Flow Field Optimisation of a Robot Vacuum Cleaner

Regular Paper

Xiao-bo Lai[1], Hai-shun Wang[1,*] and Hua-shan Liu[2]

1 College of Information Technology, Zhejiang Chinese Medical University, China
2 College of Information Science and Technology, Donghua University, China
*Corresponding author e-mail: shopo@zjtcm.net

Abstract The duct of a robot vacuum cleaner is the length of the flow channel between the inlet of the rolling brush blower and the outlet of the vacuum blower. To cope with the pressure drop problem of the duct flow field in a robot vacuum cleaner, a method based on Pressure Implicit with Splitting of Operators (PRISO) algorithm is introduced and the optimisation design of the duct flow field is implemented. Firstly, the duct structure in a robot vacuum cleaner is taken as a research object, with the computational fluid dynamics (CFD) theories adopted; a three-dimensional fluid model of the duct is established by means of the FLUENT solver of the CFD software. Secondly, with the k-ε turbulence model of three-dimensional incompressible fluid considered and the PRISO pressure modification algorithm employed, the flow field numerical simulations inside the duct of the robot vacuum cleaner are carried out. Then, the velocity vector plots on the arbitrary plane of the duct flow field are obtained. Finally, an investigation of the dynamic characteristics of the duct flow field is done and defects of the original duct flow field are analysed, the optimisation of the original flow field has then been conducted. Experimental results show that the duct flow field after optimisation can effectively reduce pressure drop, the feasibility as well as the correctness of the theoretical modelling and optimisation approaches are validated.

1. Introduction

It is known that household cleaning is a series of repeated and tedious manual tasks, carried out by thousands of people every day. Hence, in the age of rapid developments in science and technologies, how to apply these high-tech achievements to reduce the intensity of labour and improve quality of life is an important issue that should be solved by researchers. In recent years, autonomous mobile robots have come under the spotlight of many researchers[1, 2, 3, 4]. In the twenty-first century, the successful development of the robot vacuum cleaner has made possible cleaning the floor automatically. However, the pressure drop of the duct inside the robot vacuum cleaner has a significant influence on cleaning efficiency. Therefore, how to optimise the duct flow field inside the robot vacuum cleaner has become particularly important.

The duct of the robot vacuum cleaner is the length of the flow channel between the inlet of the rolling brush blower and the outlet of the vacuum blower, which also includes the dust container and other intermediaries. It has a

significant impact on the fluid dynamics performance of the entire duct system. Traditional duct design methods mainly rely on the results of a comprehensive survey to test the duct properties. One disadvantage of these approaches is that their design cycles are very long. Moreover, the testing costs of three-dimensional flow field are very high, because the duct shape is usually complex. Fortunately, the development of computational fluid dynamics provides a good way to understand the flow field distribution and the unsteady transformation of the duct for the majority of researchers. Ishtiaque et al.[5] modified the design of the transport duct and analysed the air-flow inside the transport duct with the computational fluid dynamics (CFD) software FLUENT after creating the transport duct geometry in the geometrical model software GAMBIT. Then the physical properties of finer and coarser count yarns made from modified, as well as conventional, transport ducts were compared to assess the enhancement of properties with transport duct modification. Gas-solid two-phase flow in a 180 degrees curved duct was simulated with a standard k-epsilon model, RNG (Renormalisation Group) based k-epsilon model, Low-Re k-epsilon model and an extended version of the standard k-epsilon model was adopted. It showed that the RNG based k-epsilon model predicted the flow behaviour better than other models[6]. Computational fluid dynamics (CFD) simulations are performed for convective heat and mass transfer between water surface and humid air flowing in a horizontal three-dimensional rectangular duct[7]. Moujaes and Aekula[8]present new results for numerical predictions of air flow and pressure distribution in two commonly used elbows. A k-epsilon turbulence model for high Reynolds number and k-epsilon Chen model are used for comparative purposes. To validate the CFD results, the results of two experimental papers using guided vanes are compared with a simulated vane run under the same condition. The simulations agreed reasonably well with published experimental results.

The present paper focuses on the duct flow field optimisation of the robot vacuum cleaner. The flow field analysis of original duct structure inside the robot vacuum cleaner is carried out using the computational fluid dynamics software FLUENT after creating the duct geometry in the geometrical model software Pro/Engineer. The simulations are done using the k-ε turbulence model of three-dimensional incompressible fluid. With the velocity vector plots on arbitrary plane of the duct flow field obtained, the defects of the original duct structure flow field are analysed. After that, the duct structure is modified and optimised, and the air-flow behaviour is simulated. The total flow rates of the original duct, as well as the optimised duct, are compared, and comparisons between the experimental values and the simulation values are also achieved. All

the results validate the effectiveness and correctness of the modelling in the paper.

2. Mathematical model of the duct flow field

2.1 Governing equations

The mass conservation equation states the rate of increase of mass in the fluid element is equated to the net rate of flow of mass into the element across its faces.

This yields

$$\frac{\partial \rho}{\partial t} + \frac{\partial (\rho u)}{\partial x} + \frac{\partial (\rho v)}{\partial y} + \frac{\partial (\rho w)}{\partial z} = 0, \qquad (1)$$

or in more compact vector notation

$$\frac{\partial \rho}{\partial t} + div(\rho \boldsymbol{u}) = 0, \qquad (2)$$

where ρ is the density, t is the time, $\boldsymbol{u}$ is the velocity vector. u, v, w are the components of the velocity vector $\boldsymbol{u}$ in the x-, y-, z-direction.

Eq. (2) is the unsteady, three-dimensional mass conservation at a point in a compressible fluid. The first term on the left hand side is the rate of change in time of the density. The second term describes the net flow of mass out of the element across the boundaries.

For an incompressible fluid, the density ρ is constant and Eq. (2) becomes

$$div(\boldsymbol{u}) = 0, \qquad (3)$$

or in longhand notation

$$\frac{\partial u}{\partial x} + \frac{\partial v}{\partial y} + \frac{\partial w}{\partial z} = 0. \qquad (4)$$

Newton's second law states that the rate of change of momentum of a fluid particle equals the sum of the forces on the particle. Then, the x-component of the momentum equation is found by setting the rate of change of x-momentum of the fluid particle equal to the total force in the x-direction on the element due to surface stresses plus the rate of increase of x-momentum due to sources.

This yields

$$\rho \frac{Du}{Dt} = \frac{\partial (-p + \tau_{xx})}{\partial x} + \frac{\partial \tau_{yx}}{\partial y} + \frac{\partial \tau_{zx}}{\partial z} + S_{mx}. \qquad (5)$$

It is not too difficult to verify that the *y*-component of the momentum equation is given by

$$\rho \frac{Dv}{Dt} = \frac{\partial \tau_{xy}}{\partial x} + \frac{\partial \left(-p + \tau_{yy}\right)}{\partial y} + \frac{\partial \tau_{zy}}{\partial z} + S_{my}, \qquad (6)$$

and the *z*-component of the momentum equation by

$$\rho \frac{Dw}{Dt} = \frac{\partial \tau_{xz}}{\partial x} + \frac{\partial \tau_{yz}}{\partial y} + \frac{\partial \left(-p + \tau_{zz}\right)}{\partial z} + S_{mz}, \qquad (7)$$

Where $\rho \dfrac{Du}{Dt}$, $\rho \dfrac{Dv}{Dt}$, $\rho \dfrac{Dw}{Dt}$ are the rates of increase of *x*-, *y*- and *z*-momentum per unit volume of a fluid particle. The pressure, a normal stress, is denoted by *p*. Viscous stresses are denoted by τ. The suffix notation τ_{ij} is applied to indicate the direction of the viscous stresses. The suffices *i* and *j* in τ_{ij} indicate that the stress component acts in the *j*-direction on a surface normal to the *i*-direction.

The momentum conservation law is usually expressed as the partial differencing equations of the Navier-Stokes equation in fluid dynamics. Currently, the simulation approaches of the Navier-Stokes (N-S) equations based on the Reynolds time average are used to solve the problem of the incompressible flow in projects. It can be written as follows:

$$\frac{\partial \left(\rho u_i\right)}{\partial t} + \frac{\partial \left(\rho u_i u_j\right)}{\partial x_j} = -\frac{\partial \rho}{\partial x_i} + \mu \frac{\partial^2 u_i}{\partial x_i \partial x_j} + \frac{\partial \overline{\left(\rho u_i' u_j'\right)}}{\partial x_j} + s_i, \quad (8)$$

where $-\overline{\rho u_i' u_j'}$ is the turbulent Reynolds stress, s_i is the source term. $i, j = 1, 2, 3$.

When the ρ and s_i are known, the solutions of the simultaneous equations combined Eq. (4) and Eq. (8) are not unique, $-\overline{u_i' u_j'}$ is still unknown. At the moment, additional turbulence models of these unknowns are required to make the solutions of the simultaneous equations closed. Since the software FLUENT provides a variety of turbulence models, the *k-ε* turbulence model is chosen in this paper.

2.2 Pressure correction equations

According to the mass conservation equation and momentum conservation equation, the continuity equation can be written as follows:

$$\frac{\partial \left(\rho u\right)}{\partial x} + \frac{\partial \left(\rho v\right)}{\partial y} = 0. \qquad (9)$$

Eq. (9) can be rewritten in the discretisation form as follows:

$$\left[\left(\rho uA\right)_{i+1,J} - \left(\rho uA\right)_{i,J}\right] + \left[\left(\rho vA\right)_{I,j+1} - \left(\rho vA\right)_{I,j}\right] = 0, \quad (10)$$

following the correction values in Eq. (11)

$$\begin{cases} u_{i,J} = u_{i,J}^* + d_{i,J}\left(p_{I-1,J}' - p_{I,J}'\right) \\ v_{I,j} = v_{I,j}^* + d_{I,j}\left(p_{I,J-1}' - p_{I,J}'\right) \\ u_{i+1,J} = u_{i+1,J}^* + d_{i+1,J}\left(p_{I,J}' - p_{I+1,J}'\right) \\ u_{i+1,J} = u_{i+1,J}^* + d_{i+1,J}\left(p_{I,J}' - p_{I,J+1}'\right) \end{cases}, \quad (11)$$

where

$$d_{i+1,J} = \frac{A_{i+1,J}}{a_{i+1,J}}$$
$$d_{I,j+1} = \frac{A_{I,j+1}}{a_{I,j+1}}.$$

Substitute the discretisation Eq. (11) into Eq. (10), we obtain

$$\begin{aligned}&\left[\left(\left(\rho dA\right)_{i+1,J} + \left(\rho dA\right)_{I,j+1} + \left(\rho dA\right)_{i,J} + \left(\rho dA\right)_{I,j}\right)\right] p_{I,J}' \\ &= \left(\rho dA\right)_{i+1,J} p_{I+1,J}' + \left(\rho dA\right)_{i,J} p_{I-1,J}' + \left(\rho dA\right)_{I,j+1} p_{I,J+1}' + \left(\rho dA\right)_{I,j} p_{I,J-1}', \quad (12) \\ &+ \left[\left(\rho u^*A\right)_{i,J} - \left(\rho u^*A\right)_{i+1,J} + \left(\rho v^*A\right)_{I,j} - \left(\rho v^*A\right)_{I,j+1}\right]\end{aligned}$$

Eq. (12) can be simplified to

$$a_{I,J} p_{I,J}' = a_{I+1,J} p_{I+1,J}' + a_{I-1,J} p_{I-1,J}' + a_{I,J+1} p_{I,J+1}' + a_{I,J-1} p_{I,J-1}' - b_{I,J}', \quad (13)$$

where

$$a_{I+1,J} = \left(\rho dA\right)_{i+1,J}$$
$$a_{I-1,J} = \left(\rho dA\right)_{i,J}$$
$$a_{I,J+1} = \left(\rho dA\right)_{I,j+1}$$
$$a_{I,J-1} = \left(\rho dA\right)_{I,j}$$
$$a_{I,J} = a_{I+1,J} + a_{I-1,J} + a_{I,J+1} + a_{I,J-1}$$
$$b_{I,J}' = \left(\rho u^*A\right)_{i,J} - \left(\rho u^*A\right)_{i+1,J} + \left(\rho v^*A\right)_{I,j} - \left(\rho v^*A\right)_{I,j+1}$$

The PRISO algorithm, which stands for Pressure Implicit with Splitting of Operators[9, 10, 11], is a pressure-velocity calculation procedure developed originally for non-iterative computation of unsteady compressible flows. PRISO involves one predictor step and two corrector steps, and may be seen as an extension of SIMPLE, with a further corrector step to enhance it. The PRISO algorithm solves the pressure correction equation twice so the method requires additional storage for calculating the

source term of the second pressure correction equation. Although this method implies a considerable increase in computational effort, it has been found to be efficient and fast[12]. Therefore, the PRISO algorithm is adopted to simulate the fluid dynamical characteristics of the duct flow field in the robot vacuum cleaner.

3. Geometric models and boundary conditions

3.1 Geometric models

The grid models of the duct structure in the robot vacuum cleaner are shown in Fig.1, mainly including the inlet, the outlet, a rolling brush blower, a vacuum blower and a dust container. To reduce the grid number and execution time, we make some simplification without affecting the computational accuracy. However, the key components (such as the rolling brush blower, vacuum blower, wall, etc.) are modelled without making any simplification. The specific places simplified are shown below:
(1) The duct system has good sealing properties and there is no air leakage except via the inlet and the outlet.
(2) The vacuum blower is viewed as a part of the duct system and not discussed separately

First of all, the "stp" format case is imported from the software Pro/Engineer to the GAMBIT for pre-processing and a closed space computational domain is obtained. Then, the grid model after pre-processing is imported into the STAR-CCM+ to be checked. If there are no geometric errors or gaps, the required volume mesh can be generated directly. The block method is adopted to meshing and the whole geometric model is divided into multi-blocks. Among them, part of the rolling blower and the vacuum blower are meshed with the unstructured grid to meet the complicated surface structures of the rotating blades. The internal walls of the blowers are divided into two regions, including the internal regions and external regions. The former contain the blades, rotating shaft and surrounded fluid regions. The rotating coordinate frame is applied to the calculation process in these regions and the speed equals the actual speed of the

blades. Other areas are also divided into several blocks and meshed with the structured grids to improve the computational efficiency. The latter comprises the outer wall of the blowers and areas around them, using the fixed coordinate frame in the calculation process. The total grid number of the duct model in the robot vacuum cleaner generated is about 105 million in the paper.

3.2. Boundary conditions

The physical parameters of the fluid regions and the solid regions (such as fluid density, etc.) are constants and the fluid flow in the duct is steady-state flow, namely, the pressure, together with the temperature does not change with time. The fluid flow medium is air and the atmospheric pressure of the experimental environment is one standard atmospheric pressure, namely, P = 101325Pa, temperature T = 295K, air density ρ = 1.25kg/m^3, air viscosity μ = 1.79×10^{-5}N · s/m^2. The duct inlet is defined to the flow inlet so that the data can be obtained from experiments the duct outlet is defined to the pressure outlet. Suppose that the speed of the fluid in the duct inlet is uniform, in which the direction is perpendicular to the border, and the back pressure of the duct outlet is zero. The number of the blades on the rolling brush blower is 6, and the rotation direction is counter clockwise with the speed of 700rpm. The number of the blades on the vacuum blower is 5 and the rotation speed is 15000rpm.

Since the air flow in the duct is not very large, the compressibility of the air has little influence on the flow behaviour of the fluid and the pressure distribution. Hence, it can be assumed that the air is incompressible and the density is constant. In this paper, the solution algorithm to the pressure-velocity coupling is the PRISO method, the convection-diffusion problems are analysed with the standard second order upwind differencing scheme. Considering the design requirements of the duct in the robot vacuum cleaner, the convergence condition to be determined is that the errors of all the physical quantities should be less than 1×10^{-5}.
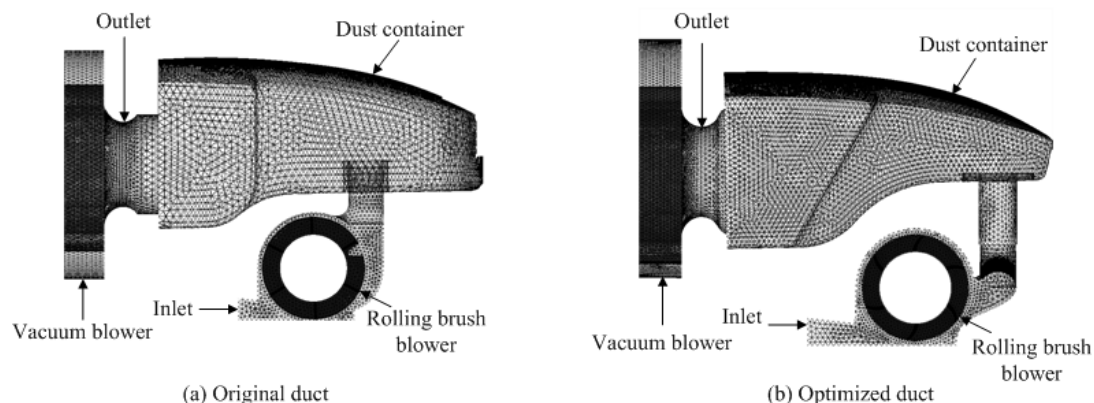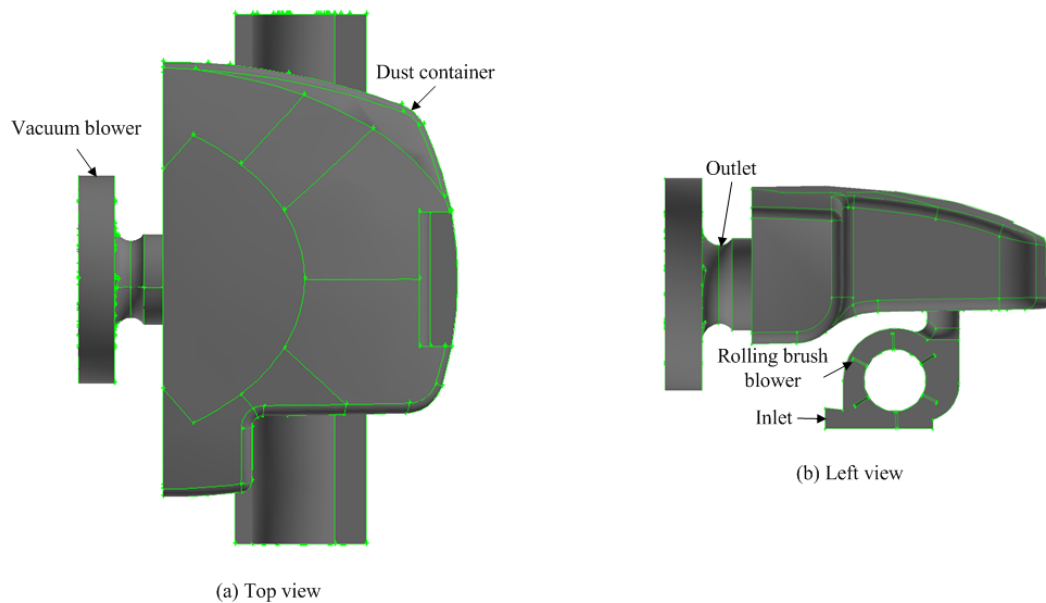

Figure 1. Grid models

(a) Top view

(b) Left view

Figure 2. 3D model of original duct structure

4. Simulation and experimental results analysis

4.1 CFD simulation of the original duct structure

The fluid model shown in Fig.2 is based totally on the design dimensions of the original duct structure in the robot vacuum cleaner, which was generated without making any changes except the simplifications. The working principle of the robot vacuum cleaner can be seen from Fig.2. Firstly, the dust particles on the ground are stirred and raised by the rotating blades of the rolling brush; then they enter the negative pressure cavity formed by the blades and the cavity wall of the rolling brush. At the same time, driven by the rolling brush blades, the dust particles can conveniently rush into the junction between the rolling brush cavity and the dust container. Secondly, the vacuum blower with high-speed rotation forms a high negative pressure chamber in the dust container. Finally, the dust particles with high-speed enter the dust container and gather under the action of the filters. This prevents the dust particles going into the interior of the vacuum blower from the inlet and avoids damage to the vacuum blower.

Fig.3 shows the overall velocity vector plot on an arbitrary plane of the original duct structure in the robot vacuum cleaner, which is obtained by CFD simulation. It can be seen from the figure that there is an obvious, large eddy in the top right of the air intake of the dust container. The eddy is generated due to the ambiguity of the flow trend after the air comes into the dust container. At the same time, the air speed is specially high in the air intake of the dust container, resulting in part of the air separating in the sequent part The eddy formed in this position not only results in higher local flow loss, but would also produce a relatively large noise. In this way it reduces the cleaning efficiency of the duct in the robot vacuum cleaner.
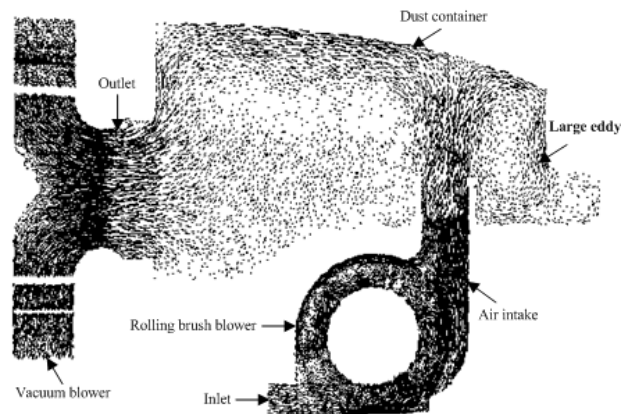
Figure 3. Velocity vector plot of the original duct structure
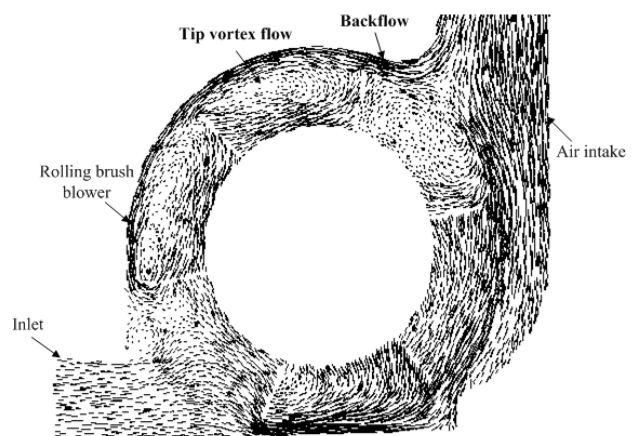
Figure 4. Rolling brush blower velocity vector plot of the original duct structure

In Fig.4, the sealing property between the top of the rolling brush blades and the rolling brush cavity is not ideal, resulting in some air along the rotation direction of the rolling brush blades leaking into the rolling brush

cavity from the left of the air intake of the dust container instead of entering the dust container directly from the air intake of the duct container. This leads to a situation in which the air circulation is not ideal and does not easily form the tip vortex flow and the backflow. Therefore, the original structure should be optimised and improved.

4.2 CFD simulation of the optimised duct structure

Through the above analysis, the large eddy, tip flow, backflow and other defects exist in the flow field of the original duct structure inside the robot vacuum cleaner, which have a great influence on cleaning efficiency. In the view of the computational fluid dynamics, the fluid pressure drop is largely caused by the eddy. Therefore, a large-scale, or even a small, eddy should be avoided when we design the duct structure of the robot vacuum cleaner. This means that the duct structure inside the robot vacuum cleaner should be optimised according to the theories of the computational fluid dynamics, maximally reducing the energy loss caused by the eddy.

As is shown in Fig.5, the optimisation scheme of the original duct structure in the paper is as follows:

Step 1: Minimize the space at the top right of the air intake in the dust container and add a spoiler at the air intake of the dust container so that the air can enter the dust container just inside the left, avoiding large eddy production and the pressure drop.

**Step 2**: The internal wall of the air intake in the dust container should be tangent to the top of the rolling brush blades, which plays a similar role as the jaw. Accordingly, the dust particles are stroked down and then enter the dust container from the air intake.

Step 3: To maximally eliminate the large eddy inside the duct, the air intake along the axial direction ought to be made in an eight-shape trumpet for smooth transition.

Step 4: The rolling brush blades are made into a bent shape so that they have the real blower effect

As is shown in Fig.6, the fluid model of the optimised duct structure is simulated through CFD software, the boundary conditions remain the same; the overall velocity vector plot on arbitrary plane of the duct structure can be obtained. We can see from Fig.6 that the large eddy in the top right of the dust container has been significantly reduced and effectively controlled after the duct structure is optimised. Meanwhile, the smoothness of the rolling brush cavity transition to the air intake has been improved greatly and the field flow of the duct structure in the robot vacuum cleaner has been perfected.

Fig.7 shows that the sealing property between the top of the rolling brush blades and the rolling brush cavity wall is better than in the original duct structure, almost no air along the rotation direction of the rolling brush blades is leaking into the rolling brush cavity from the left of the air intake in the dust container. The smoothness of the air flow is good, which effectively controls the production of the tip flow and the backflow.

(a) Top view

(b) Left view
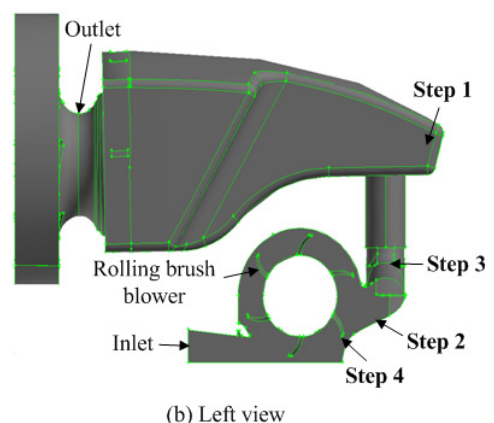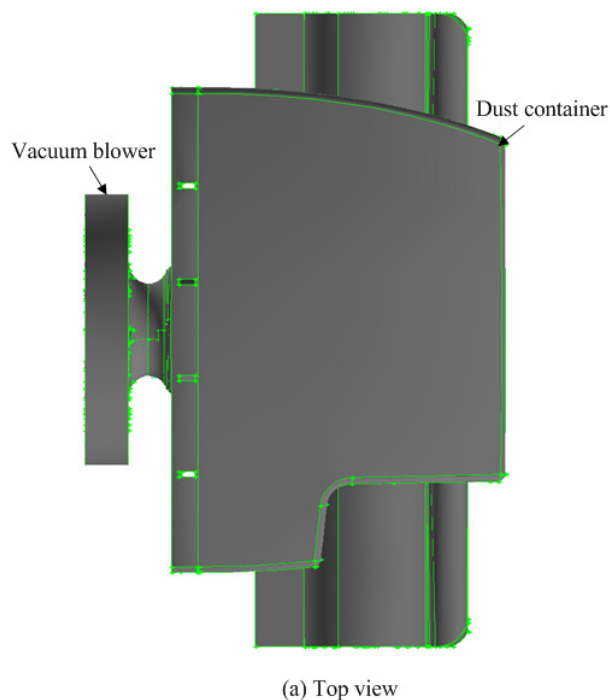
Figure 5. 3D model of the optimised duct structure
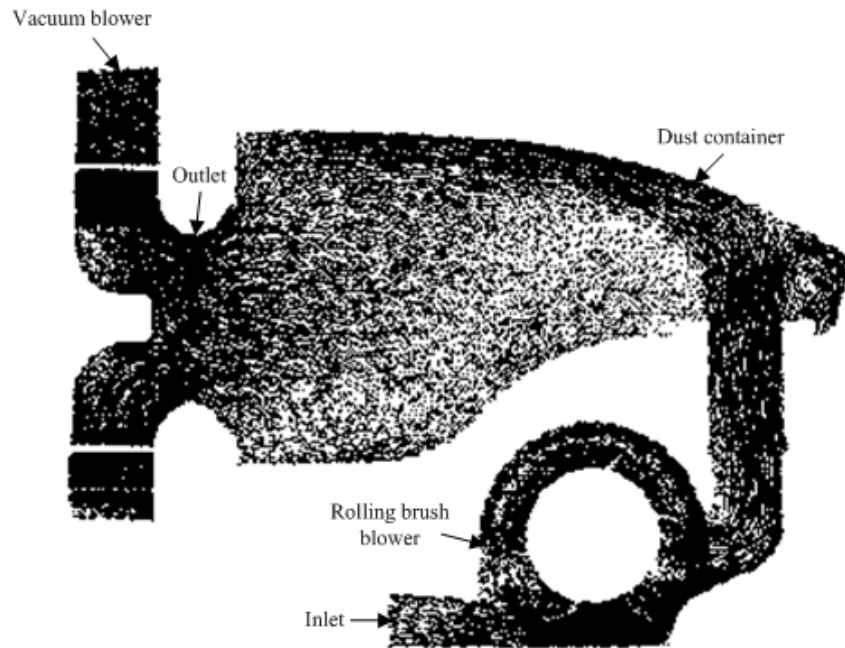
**Figure 6.** Velocity vector plot of the optimised duct structure
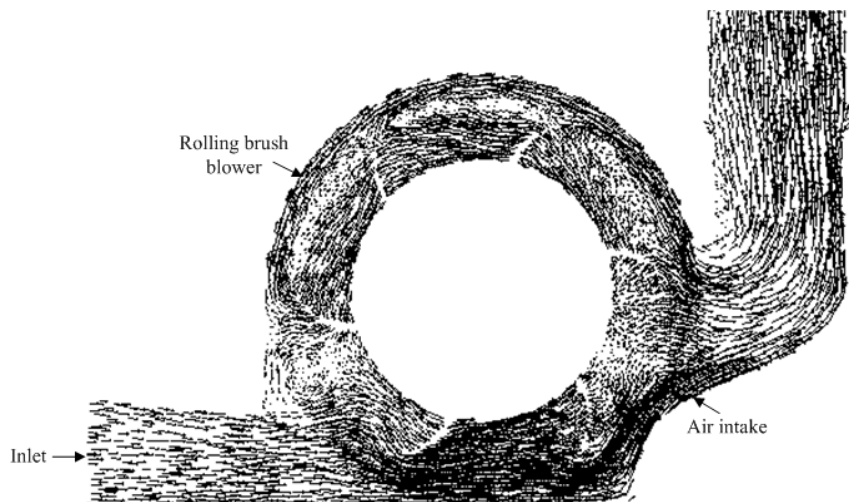
Figure 7. Rolling brush blower velocity vector plot of the optimised duct structure

4.3 Validation of calculation results

Both the original duct structure and the optimised duct structure are made into physical models and then the total air flow rate from the outlet of the vacuum blower is measured with the air flow meter. The physical model of the optimised rolling brush blades, the dust container and the air intake of the dust container are shown in Fig.8, Fig.9 and Fig.10, respectively. Table 1 shows the total air flow rate from the outlet of the original physical model and the optimised physical model under different speed conditions, respectively. The rotation speed of the rolling brush blower maintains 700rpm. It can be seen from Table 1 that the total air flow rate of the optimised physical model is larger than that of the original physical model of the duct structure with the

same speed, which verifies the correctness of the duct structure optimisation in this paper.

Fig.11 (a) shows the comparison between the experimental results and the CFD simulation results of the total air flux rate from the vacuum blower outlet of the original duct structure. Likewise, Fig.11 (b) shows the comparison between the experimental results and the CFD simulation results of the total air flux rate from the vacuum blower outlet of the optimised duct structure. All the results in Fig.11 (a) and Fig.11 (b) are tested with different rotation speeds of the vacuum blower. The data comparisons of Fig.11 (a) and Fig.11 (b) verify the correctness and the feasibility of theoretical modelling presented in the paper.
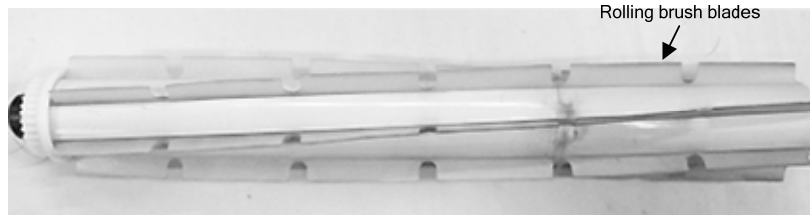
**Figure 8.** Physical model of the optimised rolling brush
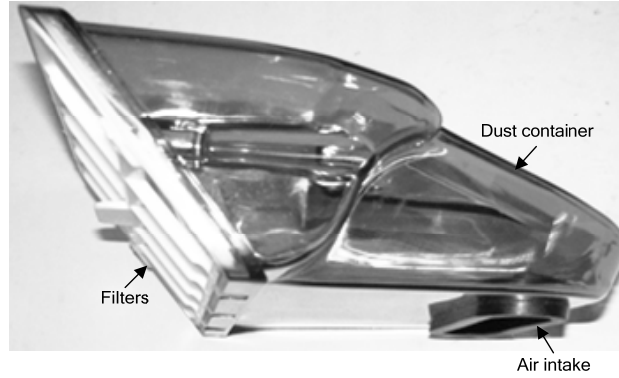
Figure 9. Physical model of the optimised dust container
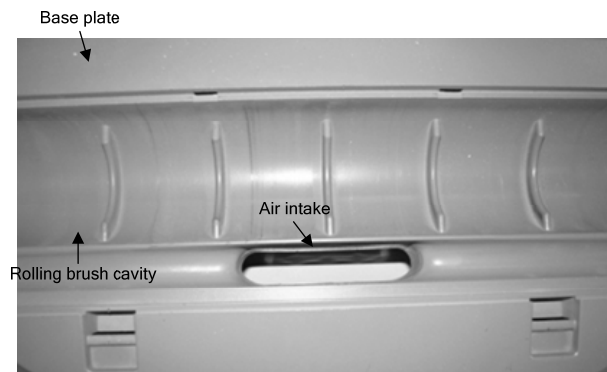
Figure 10. Physical model of the optimised air intake

Rotate speed	10000/rpm	12000/rpm	14000/rpm	16000/rpm
Original structure	49.3/(m³. h⁻¹)	54.1/(m³. h⁻¹)	60.9/(m³. h⁻¹)	66/(m³. h⁻¹)
Optimised structure	52/(m³. h⁻¹)	56.5/(m³. h⁻¹)	61/(m³. h⁻¹)	69.3/(m³. h⁻¹)

Table 1. Comparison of total air flow rate from the vacuum blower outlet at different speeds
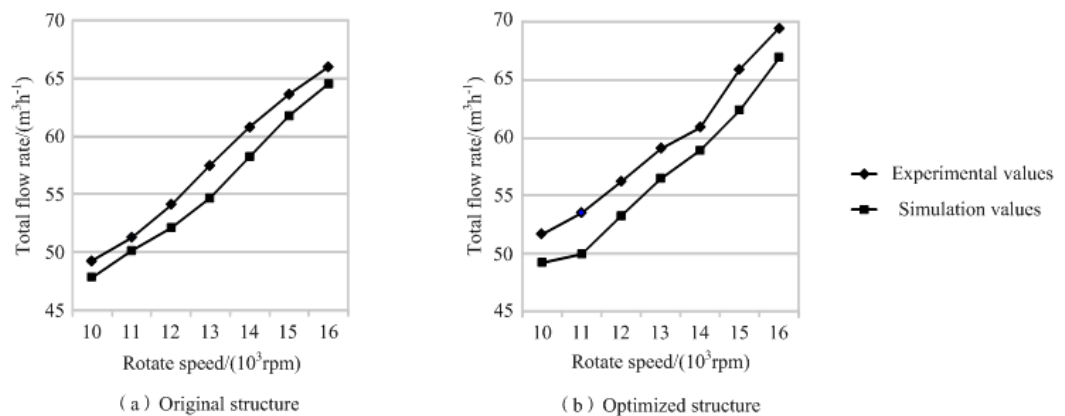
Figure 11. Total air flow rate comparison between experimental values and simulation values

5. Conclusions

Aiming at the pressure loss problem of the duct flow field in the robot vacuum cleaner, by means of computational fluid dynamics and aerodynamics, with the mass conservation equation and momentum conservation equation considered, the duct structure inside the robot vacuum cleaner is taken as a research object in this paper. The convection-diffusion problems are analysed with the standard second order upwind differencing scheme and the k-ε turbulence model of 3D incompressible fluid and the PRISO algorithm are used to carry out the flow field numerical simulations of the duct structure in the robot vacuum cleaner. To obtain good dynamic performance, optimisation design based on the analysed results is achieved. The experimental and simulation results show that the method of optimising the duct structure inside the robot vacuum cleaner can effectively reduce the impact on the duct flow field introduced by the large eddy, tip eddy and backflow. The pressure drop is decreased and the cleaning efficiency of the robot vacuum cleaner is improved. What is more, the correctness and the feasibility of theoretical modelling presented in the paper are verified, which can overcome the shortcomings of the duct traditional design method. The conclusions obtained from this paper provide a useful reference and practical significance to the research on the aerodynamics characteristics of the duct flow field in other robots.

6. References

[1] Hong J., Park K.. A new mobile robot navigation using a turning point searching algorithm with the consideration of obstacle avoidance. *International Journal of Advanced Manufacturing Technology*, 2011, 52(5-8): 763-775. [doi: 10.1007/s00170-010-2749-5]

[2] Klancar G., Matko D., Blazic S.. A control strategy for platoons of differential drive wheeled mobile robot. *Robotics and Autonomous Systems*, 2011, 59(2): 57-64. [doi: 10.1016/j.robot.2010.12.002]

[3] Samsudin K., Ahmad F. A., Mashohor S.. A highly interpretable fuzzy rule base using ordinal structure for obstacle avoidance of mobile robot. *Applied Soft Computing*, 2011, 47(1): 85-91. [doi: 10.1016/j.asoc.2010.05.002]

[4] Matveev A. S., Teimoori H., Savkin A. V.. Navigation of a unicycle-like mobile robot for environmental extremum seeking. *Automatica*, 2011, 47(1): 85-91. [doi: 10.1016/j.automatica.2010.10.003]

[5] Ishtiaque S. M., Singh S. N., Das A., et al. Optimisation of fluid flow phenomena inside the transport duct of a DREF-◎ friction spinning machine. *Journal of the Textile Institute*, 2010, 101(10): 906-916. [doi: 10.1080/00405000903028240]

[6] EI-Behery S. M., Hamed M. H., EI-Kadi M. A., et al. CFD prediction of air-solid flow in 180 degrees curved duct. *Powder Technology*, 2009, 191(1-2): 130-142. [doi: 10.1016/j.powtec.2008.09.018]

[7] Talukdar P., Iskra C. R., Simonson C. J.. Combined heat and mass transfer for laminar flow of moist air in a 3D rectangular duct: CFD simulation and validation with experimental data. *International Journal of Heat and Mass Transfer*, 2008, 51(11-12): 3091-3102. [doi: 10.1016/j.ijheatmasstransfer.2007.08.034]

[8] Moujaes S. F., Aekula S.. CFD predictions and experimental comparisons of pressure drop effects of turning vanes in 90 degrees duct Elbows. *Journal of Energy Engineering-ASCE*, 2009, 135(4): 119-126. [doi: 10.1061/(ASCE)0733-9402(2009)135:4(119)]

[9] Issa R. I.. Solution of the implicitly discretised fluid flow equations by operator-splitting. *Journal of Computational Physics*, 1986, 62(1): 40-65. [doi: 10.1016/0021-9991(86)90099-9]

[10] Park TS. Effects of time-integration method in a large-eddy simulation using the PISO algorithm: Part I - Flow field. *Numerical Heat Transfer Part A-Applications*, 2006, 50(3): 229-245. [doi: 10.1080/10407780600602374]

[11] Kang KG, Ryou HS. Computation of solidification and melting using the PISO algorithm. *Numerical Heat Transfer Part B-Applications*, 2004, 46(2): 179-194. [doi:10.1080/10407790490438563]

[12] Issa R. I., Gosman A. D., Watkins A. P.. The computation of compressible and incompressible recirculating flows. *Journal of Computational Physics*, 1986, 62(1): 66-82. [doi: 10.1016/0021-9991(86)90100-2]